



Topological entropy and the controlled effect of glucose in the electrical activity of pancreatic β -cells

Jorge Duarte ^{a,*}, Cristina Januário ^a, Nuno Martins ^b

^a ISEL-High Institute of Engineering of Lisbon, Department of Chemistry, Mathematics Unit, Rua Conselheiro Emídio Navarro, 1949-014 Lisboa, Portugal

^b Department of Mathematics, Centre of Mathematical Analysis, Geometry and Dynamical Systems, Instituto Superior Técnico, Av. Rovisco Pais 1, 1049-001 Lisboa, Portugal

ARTICLE INFO

Article history:

Received 22 October 2008

Received in revised form

28 July 2009

Accepted 12 August 2009

Available online 21 August 2009

Communicated by G. Stepan

PACS:

89.65.Gh

89.70.Cf

89.75.Fb

05.45.Ac

Keywords:

Pancreatic β -cells

Glucose

Bursting activity

Kneading theory

Topological entropy

Chaos control

ABSTRACT

Insulin secretion from electrically coupled β -cells is governed by bursting electrical activity. In response to stimulatory concentrations of glucose, the membrane potential of pancreatic β -cells may experience a transition from bursting-spiking oscillations to continuous spiking oscillations. This transition can be chaotic but becomes more and more regular with an increase in glucose. In the presence of chaos, the inability to predict the behavior of dynamical systems suggests the application of chaos control methods, when we are more interested in obtaining attracting time periodic motion. In this article, we focus our attention on a specific mathematical model from the literature that mimics the glucose-induced electrical activity of pancreatic β -cells (Deng, 1993 [7]). Firstly, using results of symbolic dynamics, we characterize the topological entropy and the parameter space ordering of the kneading sequences, associated with one-dimensional maps that reproduce significant aspects of the model dynamics. The analysis of the variation of this numerical invariant allows us to quantify and to distinguish different chaotic regimes. Finally, we show that chaotic orbits of the system can be controlled, without changing their orbital properties, and be turned into desired limit cycles. The control is illustrated by an application of a feedback control technique developed by Romeiras, Grebogi, Ott and Dayawansa (1992) [13]. This work provides an illustration of how our understanding of biophysically motivated models can be directly enhanced by the theory of dynamical systems.

© 2009 Elsevier B.V. All rights reserved.

1. Motivation and preliminaries

Pancreatic β -cells are a well-studied example of emergent oscillations in interacting cell populations. The β -cells are organized into functional units of thousands of endocrine cells, called islets of Langerhans. In the presence of a stimulatory level of glucose, the membrane potential of these cells exhibits bursting oscillations. Bursting consists of alternating active and silent phases of spiking and quiescence, respectively. The bursting mechanism was first identified by Rinzel in [1], whose particular form seen in β -cells is essentially of “square wave” (see [2] and [3]). The electrical activity is of the utmost importance for the biophysical function of the cells because it governs oscillations in the intracellular calcium concentration, the trigger for the release of the hormone insulin.

One of the first models for bursting was proposed by Atwater et al. [4]. It was based on extensive experimental data, incorporating the important cellular mechanisms that were thought to underlie bursting. Following this experimental work, Chay and Keizer developed a mathematical model for the ionic and electrical behavior of the pancreatic β -cells [5]. This model was reduced to a system of three variables and studied in terms of chaotic dynamics by Chay [6]. There are several revised and refined models proposed by many researchers based on the Chay–Keizer model, but the qualitative mechanism for the bursting oscillations is the same.

In order to study a geometrical mechanism for chaos generation, Bo Deng introduced a system that reproduces phenomenologically the glucose-induced electrical activity on the pancreatic β -cells [7]. The experimental data were regenerated mathematically and consists of six time series recordings taken from [8]. They were obtained experimentally by the technique of microelectrode recording. The researchers impaled a β -cell within an islet of Langerhans and measured the collective glucose-induced electrical activity of around 1000 cells. In [9], Bo Deng proved the existence of one-dimensional Poincaré return maps generated by the model and left open a collection of questions pertaining to chaotic

* Corresponding author.

E-mail addresses: jduarte@deq.isel.ipl.pt (J. Duarte), cjanuario@deq.isel.ipl.pt (C. Januário), nmartins@math.ist.utl.pt (N. Martins).

attractors in terms of symbolic dynamics and various measurements of complexity (see [7,9]).

In recent years, there has been a considerable research effort into the analysis of chaotic systems. For instance, control, targeting, synchronization and forecasting of chaotic motion have proved well-established results in the fields of physics, applied mathematics and engineering. In particular, since the publication of the seminal paper of Ott, Grebogi and Yorke in 1990 [10], there has been a great deal of progress in the development of techniques for the control of chaotic phenomena, with applications, for example, to physiology, biochemistry, cardiology, communications, physics laboratories and turbulence. Indeed, the dynamical control of cardiac [11] and neuronal tissues [12] has been one of the most practical application of chaos control techniques to biological systems. By exploiting the natural dynamics of the systems, these techniques were used to stabilize or destabilize heartbeats and neuronal firing with minimum perturbation. The central question addressed in the theory of chaos control is: *given a chaotic system, how can we obtain improved performance and achieve a desired attracting time-periodic motion by making small controlling temporal perturbations in an accessible system parameter?* [13].

In the context of the electrical activity of β -cells, irregular bursting and spiking solutions of some representative biophysical models can be converted efficiently to periodic spike trains (regular beating and periodic bursting), using practical methods of the new and exciting field of chaos control. Particularly, in order to control the chaotic motion, we do not need to change the fundamental characteristics of the system; we only have to impose upon the dynamics some small perturbations. The application of small external adjustment to the model leaves the main features unchanged and is able to eliminate chaotic bursts.

The goal of our article is to provide a contribution for the detailed analysis of the chaotic behavior of the Deng model, which is cast as a singularly perturbed system of ordinary differential equations, through a comprehensive study of a family of unimodal Poincaré return maps (logistic-like maps) presented in [9], which incorporates fundamental dynamical properties of the three-dimensional attractor.

In fact, we can gain some significant qualitative insights into the principles and mechanisms underlying chaotic bursting behavior by studying low-dimensional maps that incorporate representative dynamical properties of the phenomenon.

A quantifier for the complex orbit structure—an attribute used to define chaos—is the topological entropy. This measure of the amount of chaos in a dynamical system is the most important numerical invariant related to the orbit growth, and its variation with particular parameters gives us a finer distinction between states of complexity. The topological entropy can be efficiently used to examine the complex behavior and to perform chaos control strategies.

In this work, we are going to exhibit an application of the pole placement technique, initially proposed by Romeiras et al. ([13]) as an extension of the Ott–Grebogi–Yorke (OGY) method carried out in [10]. As far as our study is concerned, this method is applied to a bi-dimensional discrete time system and uses a linear approximation, obtained from the induced dynamics, in the neighborhood of the desired periodic orbit.

For the sake of clarity, we describe briefly the main aspects of the Deng model considered (for additional details the reader is referred to [7,9]).

The phenomenological Deng model that mimics the glucose-induced electrical activity on pancreatic β -cells is given by the following differential system:

$$\frac{dC}{dt} = \epsilon(V - \rho)$$

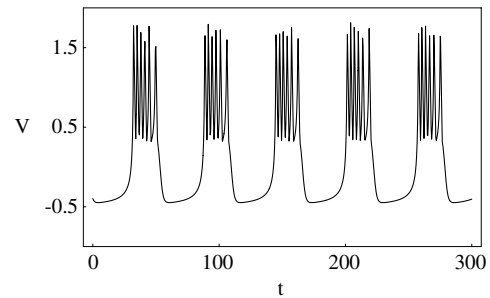


Fig. 1. The V -profile (action potentials) of a bursting-spiking orbit for system (1).

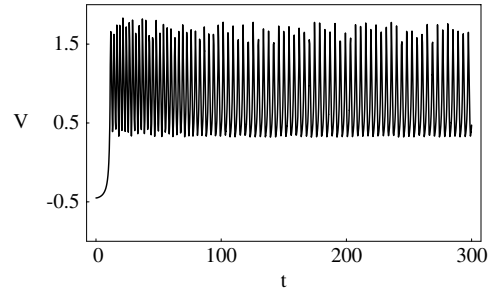


Fig. 2. The V -profile (action potentials) of a continuous spiking orbit for system (1).

$$\begin{aligned} \zeta \frac{dN}{dt} &= (N - N_{\min})(N_{\max} - N) \times [(V - V_{\max}) + r_1(N - N_{\min})] \\ &\quad - \eta_1(N - r_2) \\ \frac{dV}{dt} &= (N_{\max} - N) \times [(V - V_{\min})(V - V_{\min}) \\ &\quad - r_3(C - C_{\min})) + \eta_2] - w(N - N_{\min}) \end{aligned} \quad (1)$$

with

$$\begin{aligned} r_1 &= \frac{V_{\max} - V_{spk}}{N_{\max} - N_{\min}}, & r_2 &= \frac{N_{\max} + N_{\min}}{2}, \\ r_3 &= \frac{V_{spk} - V_{\min}}{C_* - C_{\min}}. \end{aligned}$$

This system consists of three dynamical variables:

- (1) variable C corresponds to the intracellular calcium Ca^{2+} concentration;
- (2) variable N measures the percentage of open potassium channels;
- (3) variable V corresponds to the membrane voltage.

The parameters are: w , N_{\min} , N_{\max} , V_{\min} , V_{\max} , V_{spk} , C_{\min} , C_* , ρ , η_1 , η_2 , ϵ and ζ . In particular, parameter ρ increases with the increase in the glucose concentration, and η_1 , η_2 , ϵ and ζ are non-negative small parameters, which control the singular perturbation processes of the model. For further information concerning the physiological significance and meaning of the variables and parameters, the reader is referred to the papers [7,9].

Depending on the value of parameter ρ , the wave forms of the temporal behavior of variable V demonstrates two qualitatively different regimes, namely *bursting-spiking oscillations* and *continuous spiking oscillations* (see Figs. 1 and 2). The *bursting-spiking oscillations* alternate between the silent phase and the active phase. It occurs for lower values of ρ near V_{spk} .

The *continuous spiking oscillations* correlates well with insulin secretion [4], and we expect that the higher the glucose concentration, the longer the period of time a typical trajectory spends in the active phase, therefore giving way to continuous spiking. It occurs for higher values of ρ near V_{\max} .

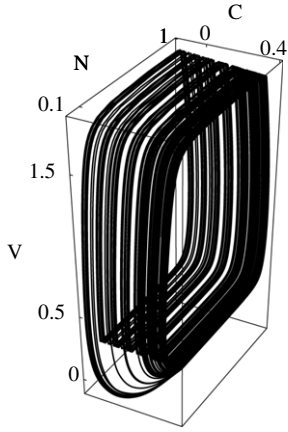


Fig. 3. Solution visualized as a trajectory in the three-dimensional space for $\rho = 0.5927$ and $\epsilon = 0.08$.

In order to illustrate the chaotic nature of the model, it is interesting to exhibit some numerical results about the behavior of the dynamical variables, namely:

- the dynamics of membrane potentials, which reveals the transition from a non-periodic to a regular mode;
- the time variation of C , which closely follows the mode of the potentials;
- iterated maps on the interval, which confirm that the irregular feature of the action potentials is indeed deterministic in nature.

2. Unimodal maps, symbolic dynamics, topological entropy and chaos

As we pointed out before, this article aims to present a comprehensive study of a family of one-dimensional maps associated with the Bo Deng biophysically motivated model. The existence of these maps, for some system realistic parameter regions (see region Ω in Fig. 13 represented below), was demonstrated in [9] using a geometric method of singular perturbations, which has proved to be extremely effective for biological models.

For numerical investigation, we will use throughout

$$\begin{aligned} w &= 1.0, & N_{\min} &= 0.0, & N_{\max} &= 1.0, & V_{\min} &= -0.5, \\ V_{\max} &= 2.0, & V_{spk} &= 0.0, & C_{\min} &= -0.5, & C_* &= 0.0, \\ \eta_1 &= 0.05, & \eta_2 &= 0.05, & \varsigma &= 0.005 \end{aligned}$$

and consider ρ and ϵ as control parameters. As we saw earlier, the parameter ρ is associated with the glucose concentration and ϵ is one of the parameters that control the singular perturbation processes of the model. In our study, we consider $0.595 \leq \rho \leq 0.8$ and $0.05 \leq \epsilon < 1$.

2.1. Return maps

Using numerical integration of the system (1), we can gain some insights into the geometry of the trajectories in the long run. After an initial transient, a structure emerges when the solution $(C(t), N(t), V(t))$ is visualized as a trajectory in three-dimensional space (Fig. 3). Some projections of the three-dimensional trajectory onto a two-dimensional plane are exhibited in Figs. 4 and 5. With the purpose of understanding the main features of the three-dimensional flow, we can construct one-dimensional maps recording the successive relative (local) maxima of the numerical solution $C(t)$, which represents the intracellular calcium concentration (see Figs. 6 and 7). These iterated maps consists of pairs (C_n, C_{n+1}) , where C_n denotes the n th local maximum. As

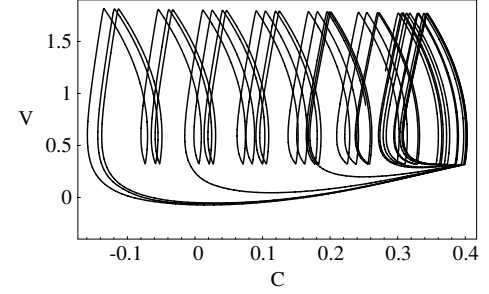


Fig. 4. Projection of the three-dimensional trajectory onto the CV -plane for $\rho = 0.5927$ and $\epsilon = 0.08$.

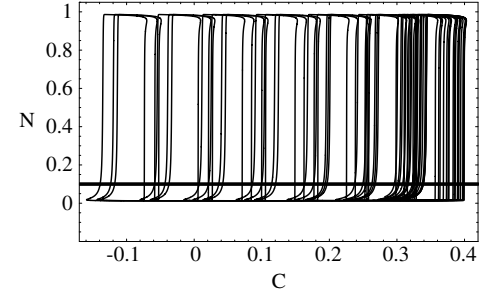


Fig. 5. Projection of the three-dimensional trajectory onto the CN -plane for $\rho = 0.5927$ and $\epsilon = 0.08$. The meaning of the bold line is assigned below.

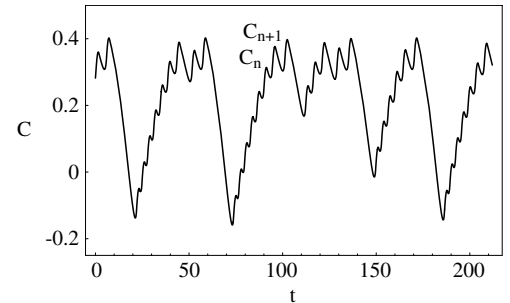


Fig. 6. Time sequence of variable C for $\rho = 0.5927$ and $\epsilon = 0.08$.

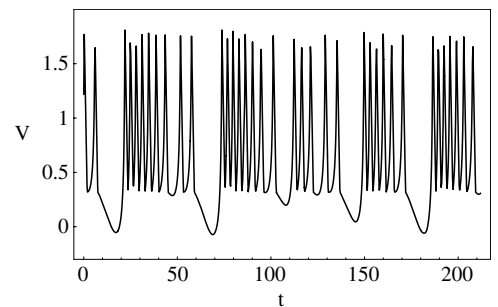


Fig. 7. Time sequence of variable V for $\rho = 0.5927$ and $\epsilon = 0.08$.

shown in Fig. 8, the data from the chaotic time series appear to fall on a logistic curve. Indeed, treating the graph as a function $C_{n+1} = f(C_n)$ allow us to reveal particularly interesting features about the dynamics on the attractor. The obtained iterated maps dynamically behave like a unimodal map, that is, continuous map on the interval with two monotonic subintervals and one turning point. In order to see the long-time behavior for different values of the control parameters ρ and ϵ at once, it is depicted in Figs. 9 and 10 typical bifurcation diagrams.

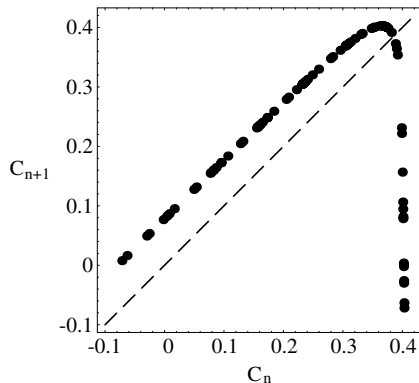


Fig. 8. The iterated map constructed from the successive local maxima of variable C ($\rho = 0.5927$ and $\epsilon = 0.08$).

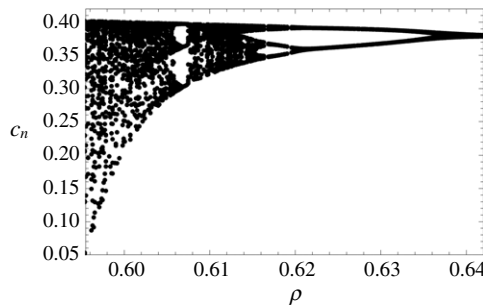


Fig. 9. Bifurcation diagram for C as a function of ρ , with $\epsilon = 0.08$ and $\rho \in [0.595, 0.62]$.

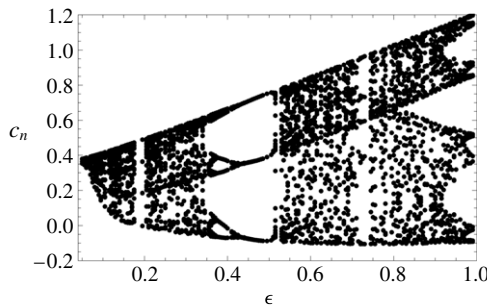


Fig. 10. Bifurcation diagram for C as a function of ϵ , with $\rho = 0.6$ and $\epsilon \in [0.05, 1]$.

2.2. Symbolic dynamics, topological entropy and chaos

At this point, we are in a position to devote our attention to the study of the topological entropy of the logistic-like maps using results of symbolic dynamics theory.

The techniques and ideas of symbolic dynamics have found significant applications. One simplification in the study of dynamical systems is to discretize time, so that the state of the system is observed only at discrete ticks of a clock, like a motion picture. This leads to the study of the iterates of a single transformation. The theory of symbolic dynamics arose as an attempt to study systems by means of discretizing space as well as time. The idea is to divide up the set of possible states into a number of pieces, and keep track of which piece the state of the system lies in at every tick of the clock. Each piece is associated with a symbol, and in this way the evolution of the system is described by a sequence of symbols. This leads to a symbolic dynamical system that helps us to understand the dynamical behavior of the original system. The paper of Milnor and Thurston [14] sets up an effective method for describing the qualitative behavior of the successive iterates of a piecewise monotonic mapping.

In what follows, we apply techniques of symbolic dynamics, in particular some results concerning to Markov partitions associated with unimodal maps. For more details see [14–16].

A unimodal map f on the interval $I = [a, b]$ is a 2-piecewise monotonic map with one critical point c . Thus, I is subdivided into the following sets:

$$I_L = [a, c[, \quad I_{C^*} = \{c\}, \quad I_R =]c, b],$$

in such way that the restriction of f to interval I_L strictly increases and the restriction of f to interval I_R decreases (see Fig. 8). Each of such maximal intervals on which the function f is monotone is called a lap of f , and the number $\ell = \ell(f)$ of distinct laps is called the lap number of f . Starting with the critical point of f , c (relative extremum), we obtain the orbit

$$O(c) = \{x_i : x_i = f^i(c), i \in \mathbb{N}\}.$$

With the purpose of studying the topological properties, we associate with the orbit $O(c)$ a sequence of symbols, itinerary $(i(x))_j = S = S_1 S_2 \dots S_j \dots$, where $S_j \in \mathcal{A} = \{L, C^*, R\}$ and

$$\begin{aligned} S_j &= L \quad \text{if } f^j(x) < c, \\ S_j &= C^* \quad \text{if } f^j(x) = c, \\ S_j &= R \quad \text{if } f^j(x) > c. \end{aligned}$$

The turning point c plays an important role since the dynamics of the interval is characterized by the symbolic sequence associated with the critical point orbit. When $O(c)$ is a k -periodic orbit, we obtain a sequence of symbols that can be characterized by a block of length k , the kneading sequence $S^{(k)} = S_1 S_2 \dots S_k C^*$.

We introduce, in the set of symbols, an order relation $L < C^* < R$. The order of the symbols is extended to the symbolic sequences. Thus, for two of such sequences P and Q in $\mathcal{A}^{\mathbb{N}}$, let i be such that $P_i \neq Q_i$ and $P_j = Q_j$ for $j < i$. Considering the R -parity of a sequence, that is, the odd or even number of occurrence of a symbol R in the sequence, if the R -parity of the block $P_1 \dots P_{i-1} = Q_1 \dots Q_{i-1}$ is even, we say that $P < Q$ if $P_i < Q_i$. And if the R -parity of the same block is odd, we say that $P < Q$ if $P_i > Q_i$. If no such index i exists, then $P = Q$.

In [14], Milnor–Thurston introduced the concept of kneading increments and kneading matrix. These are power series that measure the discontinuity evaluated at the turning points c_i , $i = 1, 2, \dots, m$, of m -modal maps. For the case of unimodal maps, we have one kneading increment defined by

$$v(t) = \theta_{c^+}(t) - \theta_{c^-}(t)$$

where $\theta_x(t)$ is the invariant coordinate of the sequence $S_0 S_1 S_2 \dots S_j \dots$ associated with the itinerary of the point x . The invariant coordinate is defined by

$$\theta_x(t) = \sum_{j=0}^{\infty} \tau_j t^j S_j,$$

where $\tau_j = \prod_{i=0}^{j-1} \varepsilon(S_i)$ for $j > 0$, $\tau_0 = 1$ for $j = 0$,

$$\varepsilon(S_i) = \begin{cases} -1 & \text{if } S_i = R \\ 0 & \text{if } S_i = C^* \\ 1 & \text{if } S_i = L \end{cases}$$

and $\theta_{c^{\pm}}(t) = \lim_{x \rightarrow c^{\pm}} \theta_x(t)$. Separating the terms associated with the symbols L and R , we obtain

$$v(t) = N_{11}(t)L + N_{12}(t)R.$$

The kneading matrix is defined by

$$N(t) = [N_{11}(t) \quad N_{12}(t)]$$

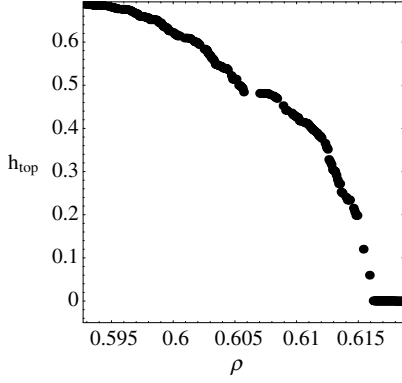


Fig. 11. Variation of the topological entropy for $\rho \in [0.595, 0.62]$ with $\epsilon = 0.08$.

and the corresponding kneading determinant, $D(t)$, is

$$\begin{aligned} D(t) &= \frac{D_1(t)}{1 - \epsilon(L)t} = -\frac{D_2(t)}{1 - \epsilon(R)t} \\ &= \frac{D_1(t)}{1-t} = -\frac{D_2(t)}{1+t}, \end{aligned}$$

where $D_1(t) = N_{12}(t)$ and $D_2(t) = N_{11}(t)$.

Now we consider the topological entropy. As we pointed out before, this important numerical invariant is related to the orbit growth and allows us to quantify the complexity of the dynamics. It represents the exponential growth rate for the number of orbit segments distinguishable with arbitrarily fine but finite precision. In a sense, the topological entropy describes in a suggestive way the total exponential complexity of the orbit structure with a single number.

A definition of chaos in the context of one-dimensional dynamical systems states that a dynamical system is called chaotic if its topological entropy is positive. Thus, the topological entropy can be computed to express whether a map has chaotic behavior, as we can see in [17,18]. In these references, Glasner and Weiss, proposed positive entropy as a property for the characterization of complex dynamical systems, more precisely, as the essential criterion of chaos. Important results were constructed using this property (please see [19,20]).

Let s be the growth number of a unimodal interval map f . The topological entropy of f , denoted by $h_{top}(f)$, is given by

$$h_{top}(f) = \log s,$$

where

$$s = \frac{1}{t^*},$$

with t^* the root of $D(t)$, which has the lowest modulus.

In order to illustrate the outlined formalism about the computation of the topological entropy, we discuss the following example.

Example 1. Let us consider the map of Fig. 8. The orbit of the turning point defines the period-12 kneading sequence RLLLLLRLRLC. The symbolic sequences that correspond to the orbits of the points c^+ and c^- are

$$\begin{aligned} c^+ &\rightarrow R(RLLLLLRLRL)^{\infty}, \\ c^- &\rightarrow L(RLLLLLRLRL)^{\infty}. \end{aligned}$$

Note that the block RLLLLLRLRL corresponds to the sequence RLLLLLRLRLC where the symbol C is replaced by R because the parity of the block RLLLLLRLRL is odd. In fact, according to the kneading theory, the shared block of the orbits of the points c^+ and c^- , RLLLLLRLRLC, must be even, that is, the symbol C is replaced

by R in order to have an even number of R symbols. The invariant coordinates are

$$\begin{aligned} \theta_{c^+}(t) &= R - Rt + Lt^2 + Lt^3 + Lt^4 + Lt^5 + Lt^6 + Lt^7 + Rt^8 \\ &\quad - Rt^9 + Lt^{10} + Lt^{11} + Rt^{12} - Rt^{13} + Lt^{14} + \dots \\ &= R - t(R - Lt - Lt^2 - Lt^3 - Lt^4 - Lt^5 - Lt^6 - Lt^7 + Rt^8 \\ &\quad - Lt^9 - Lt^{10} - Rt^{11}) - t^{13}(R - Lt - \dots - Rt^{11}) - \dots \\ &= R - t(R - Lt - Lt^2 - Lt^3 - Lt^4 - Lt^5 - Lt^6 - Lt^7 \\ &\quad + Rt^8 - Lt^9 - Lt^{10} - Rt^{11}) \times (1 + t^{12} + t^{24} + \dots) \\ &= R - t(R - Lt - Lt^2 - Lt^3 - Lt^4 - Lt^5 - Lt^6 - Lt^7 \\ &\quad + Rt^8 - Lt^9 - Lt^{10} - Rt^{11}) / (1 - t^{12}) \end{aligned}$$

and

$$\begin{aligned} \theta_{c^-}(t) &= L + Rt - Lt^2 - Lt^3 - Lt^4 - Lt^5 - Lt^6 - Lt^7 - Rt^8 + Rt^9 \\ &\quad - Lt^{10} - Lt^{11} - Rt^{12} + Rt^{13} - Lt^{14} - \dots \\ &= L + t(R - Lt - Lt^2 - Lt^3 - Lt^4 - Lt^5 - Lt^6 - Lt^7 + Rt^8 \\ &\quad - Lt^9 - Lt^{10} - Rt^{11}) + t^{13}(R - Lt - \dots - Rt^{11}) + \dots \\ &= L + t(R - Lt - Lt^2 - Lt^3 - Lt^4 - Lt^5 - Lt^6 - Lt^7 \\ &\quad + Rt^8 - Lt^9 - Lt^{10} - Rt^{11}) \times (1 + t^{12} + t^{24} + \dots) \\ &= L + t(R - Lt - Lt^2 - Lt^3 - Lt^4 - Lt^5 - Lt^6 - Lt^7 \\ &\quad + Rt^8 - Lt^9 - Lt^{10} - Rt^{11}) / (1 - t^{12}). \end{aligned}$$

The kneading increment is given by

$$\begin{aligned} v(t) &= \theta_{c^+}(t) - \theta_{c^-}(t) \\ &= R - t(R - Lt - Lt^2 - Lt^3 - Lt^4 - Lt^5 \\ &\quad - Lt^6 - Lt^7 + Rt^8 - Lt^9) / (1 - t^{12}) \\ &\quad - (L + t(R - Lt - Lt^2 - Lt^3 - Lt^4 - Lt^5 - \\ &\quad - Lt^6 - Lt^7 + Rt^8 - Lt^9) / (1 - t^{12})) \\ &= \left(-1 + \frac{2t^2 + 2t^3 + 2t^4 + 2t^5 + 2t^6 + 2t^7 + 2t^{10} + 2t^{11}}{1 - t^{12}} \right) L \\ &\quad + \left(1 + \frac{-2t + 2t^8 - 2t^9 + 2t^{12}}{1 - t^{12}} \right) R \end{aligned}$$

and the kneading matrix, $N(t)$, is such that

$$[N(t)]^T = \begin{bmatrix} -1 + \frac{2t^2 + 2t^3 + 2t^4 + 2t^5 + 2t^6 + 2t^7 + 2t^{10} + 2t^{11}}{1 - t^{12}} \\ 1 + \frac{-2t + 2t^8 - 2t^9 + 2t^{12}}{1 - t^{12}} \end{bmatrix}^T.$$

Since $D(t) = \frac{D_1(t)}{1-t} = -\frac{D_2(t)}{1+t}$, we obtain

$$D(t) = \frac{1 - 2t + 2t^8 - 2t^9 + t^{12}}{(1-t)(1-t^{12})}.$$

Therefore, $t^* = 0.502140\dots$ and the topological entropy is given by

$$h_{top}(f) = \log \left(\frac{1}{t^*} \right) = 0.688874\dots$$

We plot in Figs. 11 and 12, the variation of the topological entropy with each of the parameters. As we can observe, there are large parameter intervals where the dynamic of the Bo Deng system is chaotic. It is interesting to notice that with the study of the kneading sequences it is possible to represent the curves, in the parameter space, corresponding to the periodic orbits of the turning point C. The diagram of Fig. 13 shows how the periods ($n \leq 5$) are organized throughout the parameter space considered (whose

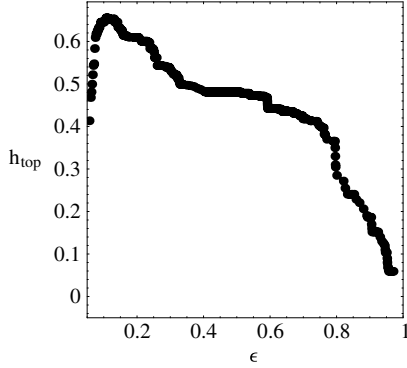


Fig. 12. Variation of the topological entropy for $\epsilon \in [0.05, 1]$ with $\rho = 0.6$.

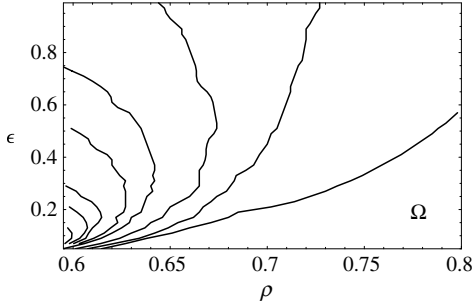


Fig. 13. Periodic orbits ($n \leq 5$) of the turning point C in the parameter region. From right to left, the corresponding kneading sequences are: C^∞ , $(RC)^\infty$, $(RLRC)^\infty$, $(RLRRC)^\infty$, $(RLC)^\infty$, $(RLLRC)^\infty$, $(RLLC)^\infty$ and $(RLLL)^\infty$.

pairs of values (s, r) correspond to logistic-like Poincaré return maps). From right to left in Fig. 13, the corresponding kneading orbits are: 1-period— C^∞ , 2-period— $(RC)^\infty$, 4-period— $(RLRC)^\infty$, 5-period— $(RLRRC)^\infty$, 3-period— $(RLC)^\infty$, 5-period— $(RLLRC)^\infty$, 4-period— $(RLLC)^\infty$ and 5-period— $(RLLL)^\infty$. The parameter space ordering of the kneading sequences leads to the identification of different levels for the topological entropy, which remains constant over each curve. The following scheme represents some kneading sequences and the corresponding topological entropy.

Kneading sequences	Root of $D(t), t^*$	Topological entropy
RC	1	0
$RLRC$	1	0
$RLRRC$	0.660992...	0.414013...
RLC	0.618034...	0.481212...
$RLLRC$	0.579639...	0.543535...
$RLLC$	0.543689...	0.609378...
$RLLL$	0.51879...	0.656256...

This is an example of how our understanding of the parameter space can be enhanced by the techniques of symbolic dynamics.

3. Control of the glucose-induced chaotic bursting oscillations in pancreatic β -cells

We begin by pointing out that the continuous time dynamics of the Deng model can be discretized via a Poincaré section, which reduces, by one unity, the dimension of the phase space. Now, we briefly describe the construction of a Poincaré map.

Consider a n -dimensional system $\frac{dx}{dt} = f(x)$. Let P be a $(n-1)$ -dimensional surface, called a Poincaré section. P is required to be transverse to the flow. We define a Poincaré map T from P to itself, obtained by following trajectories from one intersection with P to the next. If $x_n \in P$ denotes the n th intersection, then the Poincaré map is defined by $x_{n+1} = T(x_n)$. In our particular case,

we have a system with three dynamical variables C, N and V . Since the control is usually designed for parameter values, where the system is known to exhibit chaotic motion, we fix, for illustrative purposes, the parameter values $\rho = 0.5927$ and $\epsilon = 0.08$, where the system's attractor exhibits positive topological entropy (see Example 1). We consider a Poincaré plane of the form $N = k$, $k \in \mathbb{R}$, namely, $N = 0.1$ (see bold line in Fig. 5). We record the successive intersections of the trajectory with the plane, which are specified by two coordinates: C_n and V_n . This is the discrete map which we are going to consider. In the next lines, we will apply the pole placement control method to the discrete Poincaré map in order to stabilize a unstable period-two orbit embedded in the chaotic attractor. By applying small adequate chosen perturbation to the dynamical system, the original chaotic trajectory can be converted into the desired stable orbit. We consider the established fixed values for the parameters, and allow the parameter ρ to vary in some small interval $|\rho - \rho_0| < \delta, \delta > 0$, around the nominal value $\rho_0 = 0.5927$, for which the map has a chaotic attractor (see Fig. 3). In the next lines, we illustrate a numerical exploration with the purpose to stabilize an unstable period-two orbit. Concerning the role and importance of periodic orbits on neuronal dynamics the author is referred to [21].

The application of the pole placement method—a numerical example

The pole placement technique (see [13,22]), which is a feedback control method, extends the OGY method, allowing for a more general choice of the so-called feedback matrix. In our attractor, the unstable period-two orbit to be stabilized is defined by two fixed points located approximately at

$$(x^{(1)}, y^{(1)}) = (0.298387, 0.647563)$$

$$(x^{(2)}, y^{(2)}) = (0.271259, 0.852426).$$

These two points verify

$$T(x^{(1)}, y^{(1)}) = (x^{(2)}, y^{(2)})$$

$$T(x^{(2)}, y^{(2)}) = (x^{(1)}, y^{(1)}).$$

The control strategy consists in finding two stabilizing local feedback control laws, which are linear maps, obtained by using least-squares fitting on the sampled data in a small neighborhood of each one of the fixed points $(x^{(1)}, y^{(1)})$ and $(x^{(2)}, y^{(2)})$. For clarity reasons, we explain the construction of a control linear law associated with one of the fixed points, for instance $(x^{(1)}, y^{(1)})$.

A stabilizing local feedback control map in a small neighborhood of the fixed point $(x^{(1)}, y^{(1)})$ is given by

$$\begin{bmatrix} x_{t+1} - x^{(1)} \\ y_{t+1} - y^{(1)} \end{bmatrix} = A_1 \begin{bmatrix} x_t - x^{(1)} \\ y_t - y^{(1)} \end{bmatrix} + B_1(\rho - \rho_0) \quad (2)$$

where

$$A_1 = \begin{bmatrix} -0.374359 & 0.0465083 \\ -0.411955 & -0.24237 \end{bmatrix}, \quad B_1 = \begin{bmatrix} 0.379974 \\ 0.927435 \end{bmatrix} \quad (3)$$

and $(\rho - \rho_0)$ is such that ρ is a parameter of the model available for small perturbations applied to the control law (2). The ergodic nature of the chaotic dynamics ensures that the state trajectory eventually enters into the neighborhood of the fixed point. Once inside, we apply the stabilizing feedback control law in order to steer the trajectory towards the desired orbit.

Now, we verify whether the system is controllable. A system is called controllable if a matrix $K_{1 \times n}$ can be found such that $A - BK$ has any desired eigenvalues. This is possible if $\text{rank}(C) = n$, where n is the dimension of the state space and C is the $(n \times n)$ matrix:

$$C = \begin{bmatrix} B : AB : A^2B : \dots : A^{n-1}B \end{bmatrix}.$$

In our case it follows that

$$C_1 = \begin{bmatrix} B_1 : A_1 B_1 \end{bmatrix} = \begin{bmatrix} 0.379974 & \vdots & -0.0991133 \\ 0.927435 & \vdots & -0.381314 \end{bmatrix} \quad (4)$$

which has rank 2, and so the system is controllable. This matrix C_1 is the *controllability matrix*.

Assume, in a small neighborhood around the fixed point $(x^{(1)}, y^{(1)})$, that

$$\rho - \rho_0 = -K \begin{bmatrix} x_t - x^{(1)} \\ y_t - y^{(1)} \end{bmatrix},$$

where $K = [k_1 \ k_2]$ is a constant vector to be determined. The linearized map becomes

$$\begin{bmatrix} x_{t+1} - x^{(1)} \\ y_{t+1} - y^{(1)} \end{bmatrix} = [A_1 - B_1 K] \begin{bmatrix} x_t - x^{(1)} \\ y_t - y^{(1)} \end{bmatrix}, \quad (5)$$

with $[A_1 - B_1 K]$ given by

$$\begin{bmatrix} -0.374359 - 0.379974 k_1 & 0.0465083 - 0.379974 k_2 \\ -0.411955 - 0.927435 k_1 & -0.24237 - 0.927435 k_2 \end{bmatrix},$$

which shows that the fixed point is then stable as long as the (2×2) -matrix $[A_1 - B_1 K]$ is asymptotically stable, that is, all its eigenvalues have modulus less than unity.

The determination of K , such that the eigenvalues of the matrix $[A_1 - B_1 K]$ have specified values is called, in the theory of control systems, *pole placement technique*. The eigenvalues λ_1 and λ_2 of the matrix $[A_1 - B_1 K]$ are called the regulator poles, and the problem of placing these poles at the desired location, by choosing K with A_1 and B_1 given, is the pole placement problem.

In our particular case, the characteristic polynomial, associated with the matrix $[A_1 - B_1 K]$, is given by

$$p(\lambda) = \lambda^2 + (0.616729 + 0.379974 k_1 + 0.927435 k_2)\lambda + (0.109893 + 0.135227 k_1 - 0.190662 k_2).$$

Since the eigenvalues verify the equations

$$\lambda_1 \lambda_2 = 0.109893 + 0.135227 k_1 - 0.190662 k_2 \quad \text{and}$$

$$\lambda_1 + \lambda_2 = -(0.616729 + 0.379974 k_1 + 0.927435 k_2),$$

the lines of marginal stability can be determined by solving the equations

$$\lambda_1 = \pm 1 \quad \text{and} \quad \lambda_1 \lambda_2 = 1.$$

These conditions guarantee that the eigenvalues λ_1 and λ_2 have modulus less than unity for k_1 and k_2 within a certain region. This region is defined by the three lines of marginal stability:

$$k_2 = 4.668508 - 0.709250 k_1,$$

$$k_2 = 0.669353 - 0.332188 k_1 \quad \text{and}$$

$$k_2 = -1.544248 - 460784 k_1.$$

We obtain stable eigenvalues considering k_1 and k_2 within the triangular region depicted in Fig. 14. Selecting, for example, $k_1 = 10.0$ and $k_2 = -4.0$ well inside the triangular region, Ω_1 , and applying the control linear law (2), we obtain the desired time periodic orbit (see Figs. 15 and 16). At this stage, it should be pointed out that depending on the values of k_1 and k_2 in the basin of attraction Ω_1 , the controlled orbit will converge towards the fixed point but take different periods of time in order to fully accomplish the convergence process. The chaotic trajectory will also converge to the desired fixed point if, in contrast, we consider fixed values of k_1 and k_2 and randomly choose some initial conditions inside the neighborhood of $(x^{(1)}, y^{(1)})$.

Theoretically, after switching on the control, the orbit continues to perform chaotic behavior for some time, unchanged from the

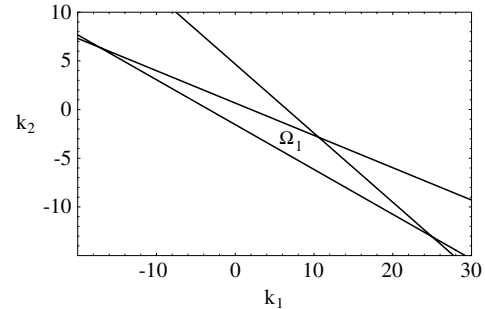


Fig. 14. The bounded region Ω_1 , related to fixed point $(x^{(1)}, y^{(1)})$, that corresponds to stable regulator poles.

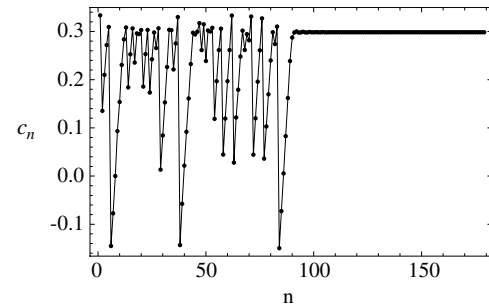


Fig. 15. Time series data for variable C_n . The control is activated in a neighborhood of the fixed point $(x^{(1)}, y^{(1)})$, after the 91th iterate.

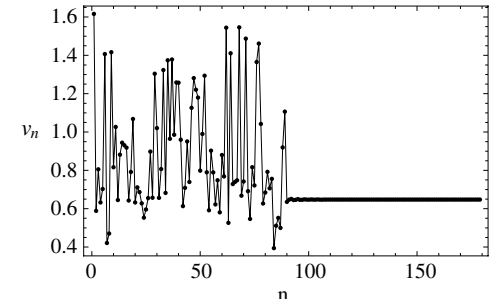


Fig. 16. Time series data for variable V_n . The control is activated in a neighborhood of the fixed point $(x^{(1)}, y^{(1)})$, after the 91th iterate.

uncontrolled case because it is not close enough to the fixed point. After some steps, this is eliminated and the orbit is rapidly brought to the fixed point.

With the same procedure used to establish the first control map, we obtain the following stabilizing local feedback law associated with the fixed point $(x^{(2)}, y^{(2)})$

$$\begin{bmatrix} x_{t+1} - x^{(2)} \\ y_{t+1} - y^{(2)} \end{bmatrix} = [A_2 - B_2 K] \begin{bmatrix} x_t - x^{(2)} \\ y_t - y^{(2)} \end{bmatrix}, \quad (6)$$

with $[A_2 - B_2 K]$ given by

$$\begin{bmatrix} 0.0276187 - 0.134076 k_1 & 0.152144 - 0.134076 k_2 \\ -0.136786 - 0.939525 k_1 & -0.05865 - 0.939525 k_2 \end{bmatrix},$$

considering k_1 and k_2 within the triangular region Ω_2 depicted in Fig. 17.

Gathering the previous information, we are able to convert efficiently the irregular dynamics arising from the chaotic coupled map to the desired period-two orbit, which is a regular spike train, by using alternately, for each iterate, Eqs. (5) and (6). Turning off the control at any stage will result in chaotic behavior which can be controlled onto another periodic motion (see Figs. 18 and 19).

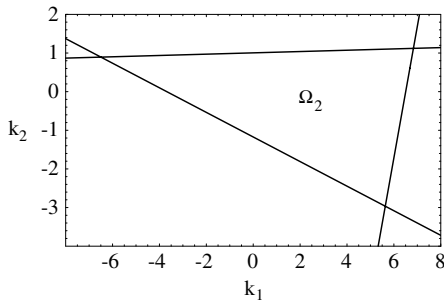


Fig. 17. The bounded region Ω_2 , related to fixed point $(x^{(2)}, y^{(2)})$, that corresponds to stable regulator poles.

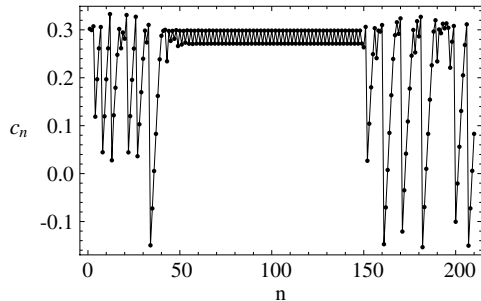


Fig. 18. Time series data for variable C_n , with and without control. The control is switched on after the 41th iterate and it is switched off after the 150th iterate.

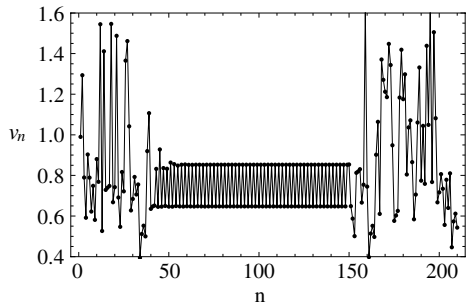


Fig. 19. Time series data for variable V_n , with and without control. The control is switched on after the 41th iterate and it is switched off after the 150th iterate.

Especially important is the fact that the control can be carried out without any need for a change to the system configuration.

In Fig. 20, we present the period-two stabilized orbit in the three-dimensional space. The corresponding time series for each variable, C and V , are depicted in Figs. 21 and 22.

4. Final considerations

In this paper, we have provided new insights into the study of the Deng model, which mimics the glucose-induced electrical activity of pancreatic β -cells. The extremely rich and complex behavior of this model allowed us to apply different theoretical and numerical approaches. More precisely, we analyzed the model in terms of symbolic dynamics theory and in terms of applicability of chaos control theory. This model addresses interesting and important mathematical and physical questions. In particular, there are no comprehensive studies about a collection of questions pertaining to chaotic behavior in terms of symbolic dynamics and measurements of complexity (see questions left open in [9]) and in terms of chaos control theory.

In the field of life sciences, where quantitatively predictive theories are rare, the use of powerful tools for the analysis of

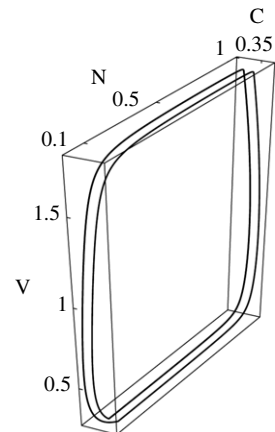


Fig. 20. The period-two stabilized orbit in the three-dimensional space.

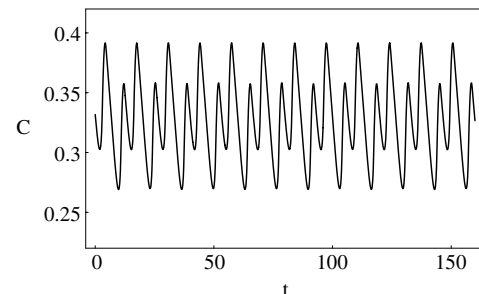


Fig. 21. Time sequence of variable C corresponding to the period-two stabilized orbit.

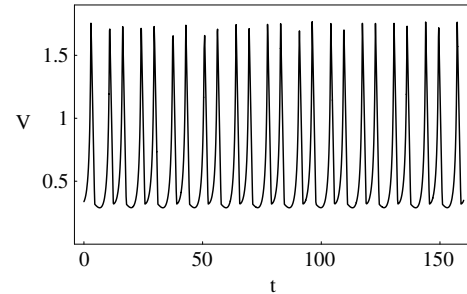


Fig. 22. Time sequence of variable V corresponding to the period-two stabilized orbit.

dynamic models, such as the symbolic dynamics theory, stands out to be extremely effective for the computation of an important numerical invariant related to the exponential orbit growth—the topological entropy.

In fact, the introduction and rigorous study of the iterated one-dimensional maps related to the calcium dynamics that incorporate the salient dynamical properties of the system became possible by analyzing the variation of this measure of complexity with the two control parameters ρ and ϵ . In all situations, the topological entropy has an absolute maximum value. This behavior is determined by the symbolic sequences ordering associated with the successive orbits of the turning point c . Our analysis reveals that the transition from bursting-spiking oscillations to continuous spiking oscillations can be chaotic but becomes more and more regular with the increase in glucose, that is, with the increase in parameter ρ .

The representation of the isentropic curves (corresponding to the periodic orbits of the turning point c) in the parameter

space allowed us to introduce the parameter space ordering of the dynamics. In fact, this construction gives insights into the behavior of the topological entropy in all the parameter space considered.

Indeed, the family of maps analyzed exhibits positive topological entropy, which demonstrates its chaotic nature. The techniques of symbolic dynamics allowed us to quantify the orbit complexity and to distinguish different chaotic regimes, extracting order from chaos, in a significant region of the parameter space.

Although chaos is unpredictable over long time periods, its deterministic nature often can be exploited by control techniques to obtain desired results. Chaos control techniques, which are "model independent" because they do not require knowledge of a system's underlying equations, have been applied successfully to a wide range of physical systems. Such success has fostered interest in applying model-independent control techniques to stabilize the fluctuations of excitable physiological systems, which are often well-understood qualitatively, but for which quantitative relationships between system components are usually incomplete. Motivated by the chaotic structure of the model, we have applied the pole placement control method in order to obtain predictable behavior—the stabilized period-two spike train. We showed, numerically, that the complicated motion that emerges from the dynamics of the coupled model can be controlled by small parameter perturbations in a control linear law. The fundamental characteristics of the model are not changed by the control procedure as the period-two orbit remains the same. We emphasize that, with the application of the chaos control technique, the model performs fast convergence for different initial conditions and different values of the control parameters. The chaotic dynamics could be converted, by using just a small feedback control, to motion on a desired periodic orbit.

Acknowledgements

The authors would like to thank Professor Bo Deng for his comments and suggestions.

References

- [1] J. Rinzel, Ordinary and Partial Differential Equations, Springer, New York, 1985.
- [2] R. Bertram, R. Butte, T. Kiemel, A. Sherman, Bull. Math. Biol. 57 (1995) 413.
- [3] J. Rinzel, Mathematical Topics in Population Biology, Morphogenesis and Neurosciences, Springer, New York, 1987.
- [4] I. Atwater, C.M. Dawson, A. Scott, G. Eddlestone, E. Rojas, The Nature of the Oscillatory Behaviour in Electrical Activity From Pancreatic Beta-cell, Georg Thieme, New York, 1980.
- [5] T.R. Chay, J. Keizer, Biophys. J. 42 (1983) 181.
- [6] T.R. Chay, Physica D 16 (1984) 233.
- [7] B. Deng, Math. Biosci. 119 (1993) 241.
- [8] A. Sherman, P. Carroll, R.M. Santos, I. Atwater, Glucose Dose Response of Pancreatic β -cells: Experimental and Theoretical Results, Transitions in Biological Systems, Plenum, New York, 1990.
- [9] B. Deng, J. Math. Biol. 38 (1999) 21.
- [10] E. Ott, C. Grebogi, J.A. Yorke, Phys. Rev. Lett. 64 (1990) 1196.
- [11] A. Garfinkel, M.L. Spano, W.L. Ditto, J.N. Weiss, Science 257 (1992) 1230.
- [12] S.J. Schiff, K. Jerger, D.H. Duong, T. Chang, M.L. Spano, W.L. Ditto, Nature 370 (1994) 615.
- [13] F.J. Romeiras, C. Grebogi, E. Ott, W.P. Dayawansa, Physica D 58 (1992) 165.
- [14] J. Milnor, W. Thurston, Lect. Notes in Math. 1342 (1988) 465.
- [15] J.P. Lampreia, J.S. Ramos, Port. Math. 54 (1997) 1.
- [16] Hao Bai-Lin, Zheng Wei-Mou, Applied Symbolic Dynamics and Chaos, in: Directions in Chaos, vol. 7, World Scientific Publishing Co., 1998.
- [17] E. Glasner, B. Weiss, Nonlinearity 6 (1993) 1067.
- [18] F. Blanchard, Topological chaos: What may this mean, arXiv:0805.0232v1[math.DS].
- [19] R. Gilmore, M. Lefranc, The Topology of Chaos, Wiley-Interscience, John Wiley & Sons, New York, 2002.
- [20] S. Ruette, Chaos for continuous interval maps—A survey of relationship between the various sorts of chaos (preprint).
- [21] P. So, J.T. Francis, T.I. Netoff, B.J. Gluckman, S.J. Schiff, Biophys. J. 74 (1998) 2776.
- [22] K. Ogata, Modern Control Engineering, Prentice-Hall, New Jersey, 1990.